Browning index: An image processing technique to aid in the segmentation of skin lesions on dermatoscopic images

Edmilson Q. S. Filho
Departamento de Engenharia Elétrica
Universidade Federal do Espírito Santo
Vitória, Brasil
edmilson.q.santos@edu.ufes.br

Evandro O. T. Salles
Departamento de Engenharia Elétrica
Universidade Federal do Espírito Santo
Vitória, Brasil
evandro.salles@ufes.br

Jacques Facon
Departamento de Computação e Eletrônica
Universidade Federal do Espírito Santo
São Mateus, Brasil
jacques.facon@ufes.br

Patrick M. Ciarelli
Departamento de Engenharia Elétrica
Universidade Federal do Espírito Santo
Vitória, Brasil
patrick.ciarelli@ufes.br

***Abstract*—Although most people believe that melanoma cancer is restricted only to skin cancer, the great danger is the spread of metastases from the skin and subcutaneous tissues to any part of the body. This justifies that early detection of cutaneous melanoma cancer remains the primary factor in reducing the mortality of this type of cancer. Currently, non-invasive segmentation-based approaches represent one of the most efficient computational frameworks when it comes to melanoma recognition. Instead of using color images directly in RGB space, as in many works in the literature, we propose the use of browning indices to highlight the differences between the skin and the area of interest to increase the recognition rates of cutaneous melanoma. Three browning indices (Aimonino, Fetuga, and Lunadei) and three segmentation techniques were evaluated in the task of cancer segmentation on a public dataset of dermatoscopic images. In addition to these indices, the U-Net network was used for the purpose of comparison and it was also evaluated combined with browning indices. The experiment rates highlighted the potential of the browning indices to better perform melanoma segmentation. U-Net obtained the Jaccard Index and F1 Score of 0.594 and 0.805, respectively, against 0.719 and 0.862 achieved by the combination of U-Net and browning indices.**

***Index Terms*—Skin Cancer, Image Processing, Browning Index, Image Segmentation, U-Net**

I. Introduction

In the world, melanoma is the most deadly form of skin cancer due to its high possibility of causing metastasis, being responsible for about 75% of deaths associated with skin cancer [1]. After this type of lesion infiltrates the lower layers of the skin, and presents a high possibility of metastasis in the most advanced stage, the chance of cure is practically non-existent. Although it is one of the less frequent types, accounting for only 1% of all cancer diagnoses, this type of lesion has the highest mortality rate.

According to the World Health Organization [2], the incidence of both non-melanoma and melanoma skin cancers has been increasing over the past decades. Currently, between 2 and 3 million non-melanoma skin cancers and 132,000 melanoma skin cancers occur globally each year [2].

Thus, early diagnosis of the disease is the main chance of cure. For this diagnosis to occur early, it is necessary that the population has access to an efficient health system. However, this does not happen easily, especially in emerging and less developed countries [2]. The only form of definitive diagnosis is to carry out a biopsy. In this procedure, part of the lesion is removed to be analyzed under the microscope by one or more pathologists with the aim of looking for cancer cells. Some exams detect skin cancer through magnifying lenses to photograph the lesion region. The diagnostic accuracy reaches 97%, avoiding unnecessary surgeries [3].

With regard to the challenge of detecting and locating skin lesions of melanoma, we can observe that both human skin and skin lesions of melanoma usually have a brownish color with different variations. It was also verified that, in the food industry, the search for color changes in food products, such as fruits, meats, among others, is of great importance to plan strategies and control these changes. And that the browning index (BI) is one of the means to measure these color changes [6].

Associating the brownish color aspects of melanoma skin lesions and the use of browning indices in the food industry, our proposal is to verify whether the use of browning indices BI can really help in the segmentation of melanoma skin lesions. And also verify if this innovation can really increase the targeting rates of melanoma skin lesions. To the best of our knowledge, only in [7] has explored the use of browning indices BI for skin cancer segmentation.

In order to assist in the early diagnosis through the analysis of lesions, this article proposes a methodology for segmenting skin melanoma cancer based on browning indices and the U-

Net deep neural network [4]. The main objective of this article is to prove that, by innovating in the use of browning color indices, it is possible to obtain segmentation rates comparable to the best segmentation rates found in the literature.

This paper is organized as follows. Section II presents a summarized knowledge about melanoma segmentation, browning index, and U-Net. Our methodology is described in Section III. in section IV we evaluate the use of browning indices with and without the U-Net network to show the potential of this type of technique for skin cancer segmentation. The experimental evaluation and analysis about the results by means of Precision, Jaccard Index, and F1 Score metrics are also described. Finally, Section V presents our conclusions and points out some future paths.

II. Methods

A. Skin Lesion Segmentation

In digital image processing and computer vision, image segmentation is the process of partitioning a digital image into image segments, which can be classified as either regions of interest or backgrounds. The goal of segmentation is to simplify, change the representation, and highlight regions of an image so that something can make sense to the analyst. More precisely, image segmentation is the process of assigning an identifier to each pixel in an image so that elements with similar characteristics can be grouped [10].

B. Browning Index

In food industries, the browning index (BI), defined as the purity of brown color, is one of the most common indicators of browning in food products containing sugar [5]. In this paper, the browning index (BI) is applied to highlight the shades of brown present in the images, thus assisting the process of segmenting the skin lesions.

Among the different browning indices available in the literature [7], three promising indices presented in Table I were chosen: $BI_{Aimonino}$ [8], $BI_{Lunadei\_2}$ [5], and BI_{Fetuga} [9].

To calculate the BIs $BI_{Aimonino}$ and $BI_{Lunadei\_2}$, the separation between the channels of the RGB image is performed. For the BI_{Fetuga}, the image is converted to the L*a*b* color space. This color system represents the quantitative relationship of colors on three axes: The L* value indicates lightness, and a* and b* are chromaticity coordinates [11]. k is a constant representing the gain applied to the red color channel (R) in the browning index $BI_{Aimonino}$. In this paper, $BI_{Aimonino}$ was used with a value of $k = 2$,as used in [7].

TABLE I: Browning indices equations [7]

Browning Index	Equation
Aimonino in RGB	$BI_{Aimonino} = kR - G - B$
Lunadei 2 in RGB	$BI_{Lunadei} = R - B$
Fetuga in L*a*b*	$BI_{Fetuga} = 100 - L$

Figure 1 depicts some melanoma images highlighted by the Aimonino, Lunadei, and Fetuga browning indices, which tend to highlight the spots with brown tones.

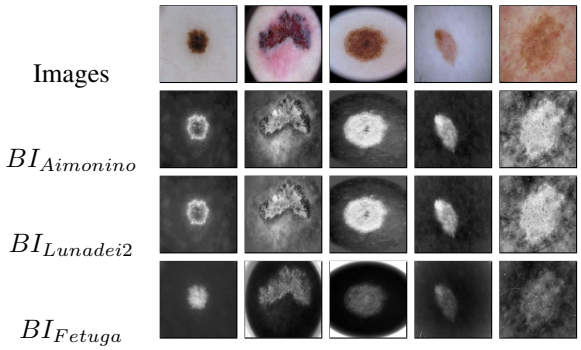

Fig. 1: Differences between skin and melanoma highlighted by different browning indices [7].

C. U-Net

The approach of a fully convolutional network was introduced in [12], in which the authors proposed an adaptation of convolutional neural networks that were used for image classification, where fully connected layers were replaced by convolutional layers. This allows a fully convolutional network to take input of any size and generate a segmented image as output. Figure 2 depicts this architecture:

- Encoder: The feature maps generated have a much lower spatial resolution than the original image. This process of reducing the spatial resolution of the input image through a series of convolutions occurs on a structure called path or also called the encoder.
- Decoder: At the encoder output, an increase in spatial resolution is made through a series of deconvolutions of the feature maps to the initial resolution of the input image. The path where this spatial resolution expansion process occurs is called the decoder or expansion path.

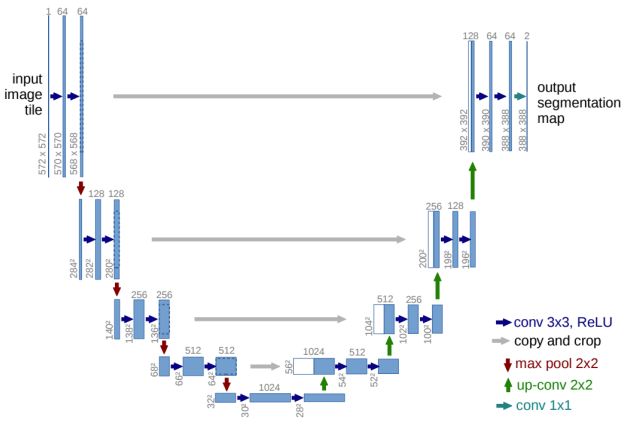

Fig. 2: The U-Net architecture is symmetric and consists of two parts: the left part is the encoder and the right part is the decoder [12].

U-Net, a network proposed in [13], is an extended version of fully convolutional networks (FCN) in order to provide more accurate segmentations with small training sets. The

main difference from FCN is in the decoder layer, where there are a large number of feature maps, having as a consequence a symmetry with respect to the encoder layer, thus taking a "U" shape, as depicted in Figure 2. The way adopted to increase the number of feature maps in the decoder is to concatenate the output of an unpooling layer with the output of the corresponding encoder convolution layer.

III. Methodology

In this section, we describe the dataset used in the experiments, the proposed strategy, the performance evaluation metrics, and the system configurations used in the simulations.

A. Dataset

The International Skin Imaging Collaboration (ISIC) is an academic and industrial partnership designed to develop research to reduce melanoma mortality. The ISIC datasets have become one of the leading repositories for researchers in machine learning for medical image analysis, especially in the field of skin cancer detection and malignancy assessment. They contain tens of thousands of dermoscopic images along with gold standard lesion diagnostic metadata [14].

The overall focus of the ISIC annual challenges is to provide support to implement autonomous algorithms for the diagnosis of melanoma through dermoscopic images. The challenges are divided into three parts corresponding to each stage of the injury analysis:

- Segmentation of lesions;
- Detection of lesion dermoscopic features;
- Classification.

The ISIC 2016 challenge dataset consists of 900 training images and 379 test images. Since it is a challenge, the ground truths of test images are not available, therefore, in this work, we only use the images from the training set. The training images are divided into 727 benign images and 173 malignant images. The input images range in size from 1024 $\times$ 768, 1022 $\times$ 767, 1504 $\times$ 1129, 2816 $\times$ 2112 and 2117 $\times$ 1988.. The focus of the present paper is on the segmentation task, so the images and their respective ground truths were used. The ground truth images are binary masks with two gray scale levels and represent the location of the lesions in the input images. Thus, they have the same dimensions as the input images. Each pixel of the ground truth images has only two values: 0, which indicates the image background or area complementary to the lesion area; 255, which indicates the main lesion.

B. Proposed strategy

The proposed strategy consists of four steps: Initially, it was decided to reproduce the experiments carried out in [7], selecting only the three browning indices and the two binarization methods considered most promising. While the three selected browning indices are $BI_{aimonino}$ with $k = 2$, $Lunadei2$ and $Fetuga$, the two binarization techniques are Otsu [15] and Lloyd [16]. Watershed [17] morphological technique has been also added. Thus obtaining nine combinations of browning indices and segmentation methods. Figure 3 depicts the flowchart from input to segmentation. In the first step, the images are resized to 256 $\times$ 256 dimension.

Fig. 3: Flowchart of the system.

In the second step, the RGB color images were processed by the deep neural network U-Net with the parameters defined in the section II-C.

The third step has consisted in evaluating the U-Net network using as input the resulting images after applying each browning index. To keep the same number of parameters of the U-Net for the different experiments, we repeated the grayscale image obtained by browning index in the tree channels of an RGB color image.

The fourth step has consisted in applying the U-Net network using as input, no longer the three RGB channels of each image, but the three browning indices $BI_{aimonino}$ with $k = 2$, $Lunadei2$ and $fetuga$. Images with the three browning indices were created. In this case, each image obtained by a kind of browning index is used as a channel in an RGB color image. An example of a new image generated by the combination of the browning indices is shown in Figure 4. As can be seen, this method provides a highlight of the region of interest, i.e., the possible lesion.

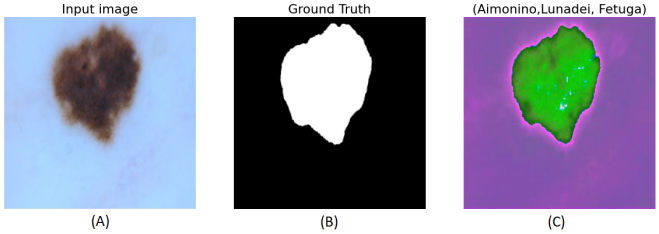

Fig. 4: (A) Input image, (B) ground truth, and (C) combined image from the BIs.

C. Performance evaluation measures

To compute the segmentation rates, the metric Accuracy, F1 Score, and Jaccard Index are normally used for evaluating the medical image segmentation task. The definitions of these metrics are presented below.

The accuracy metric is the number of correct predictions divided by the total number of predictions. Thus, this metric can be defined as:

$$Accuracy = TP + TN/(TP + TN + FN + FP). \quad (1)$$

F1 Score is the harmonic mean of precision and recall, where precision measures the quality of the model to segment correctly pixels that are from the skin lesion and recall

measures the capability of the model in identifying all pixels of the skin lesion. F1 Score combines precision and recall into a single metric for a better understanding of model performance. F1 Score is computed by the equation:

$$F1 = 2TP/(2TP + FP + FN). \quad (2)$$

Jaccard Index is the area of overlap between the predicted segmentation and the ground truth divided by the area of union between the predicted segmentation and the ground truth. Thus, this metric can be defined as:

$$Jaccard = TP/(TP + FP + FN). \quad (3)$$

In the context of skin lesion segmentation:

- TP (true positive) and TN (true negative) are pixels from a skin lesion and background (according to ground truth), respectively, which were segmented correctly;
- FP (false positive) and FN (false negative) are pixels from a skin lesion and background (according to ground truth), respectively, which were not segmented correctly.

The three metrics vary between 0 and 1, with 1 meaning the closest match between the predicted and the ground truth.

D. System configurations

All experiments were run on a Windows 10 64 bits composed of an Intel(R) Core(TM) i5-8300H CPU @ 2.30GHz 2.30 GHz and 8 GB RAM. Furthermore, the deep extractors were implemented using the Python 3.9.12 programming language, and Keras 2.1.4, a deep learning API with a Tensorflow 1.8 backend.

IV. Experiments

The data consists of 900 input images and 900 ground truth images, which were separated into 70% (630 images) for training, 15% (135 images) for validation, and 15% (135 images) for testing. The same test images were applied to all the evaluated methods.

Initially, the browning indices $BI_{aimonino}$ with $k = 2$, $Lunadei2$, and $Fetuga$ were calculated as shown in Table I. Then, the images were segmented using the methods of Otsu, Lloyd, and Watershed. As described in Section III-C, the metrics Accuracy, Jaccard Index, and F1-Score were used to quantify the results of the proposed models and compare the performance between them.

The architecture of the used U-Net consists of a contracting path and an expansive path. The contracting path follows the typical architecture of a convolutional network. It consists of the repeated application (five times) of two 3×3 convolutions, each followed by a rectified linear unit (ReLU) and a 2×2 max pooling operation with stride 2 for downsampling. At each downsampling step, we double the number of feature channels. Every step in the expansive path consists of an upsampling of the feature map followed by a 2×2 convolution that halves the number of feature channels, a concatenation with the correspondingly cropped feature map from the contracting path, and two 3×3 convolutions, each followed by a ReLU. At the final layer, a 1×1 convolution is used to map each 64-component feature vector to the desired number of classes. In total, the network has 23 convolutional layers.

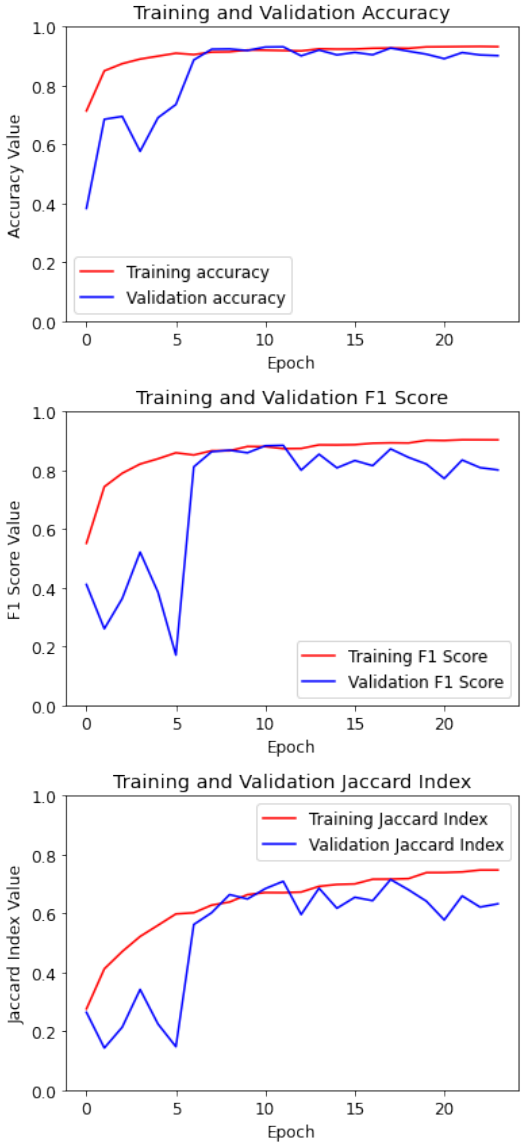

Fig. 5: Results of the 25 epochs of image segmentation tasks for the best case made of the (Aimonino, Fetuga, and Lunadei) combination.

The training of the U-Net was carried out using the hyperparameters of Table II. The binary cross entropy function was chosen to minimize losses during the training since it is commonly used to quantify the difference between two probability distributions. The optimizer used was Adaptive Moment Estimation (Adam), which is an adaptive learning rate method. The early stop technique was applied, which consists of setting a patience value for the network to show improvement. If there is no improvement after a certain number of epochs (the patience value), the model stops training and uses the parameters that obtain the best results.

The graphics in Figure 5 present the results of 25 epochs

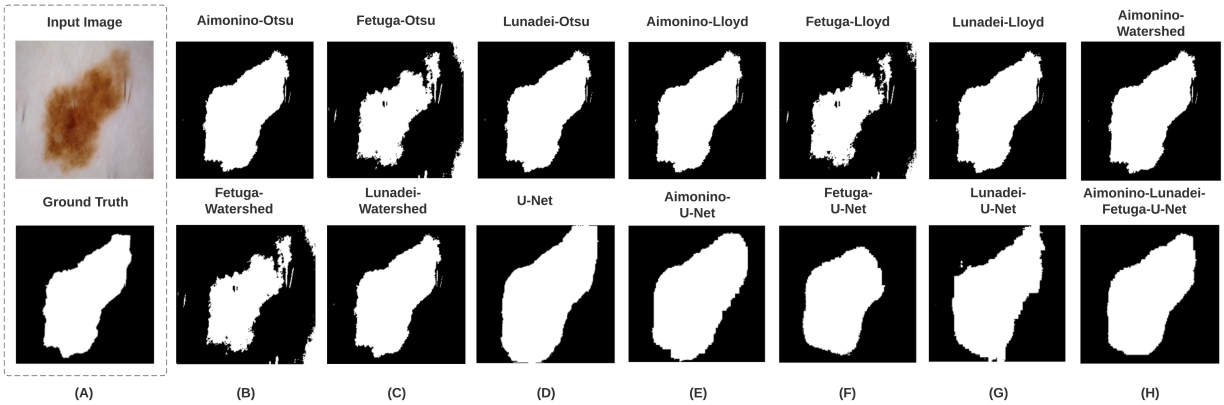

Fig. 6: In column (A) is shown the input image and its ground truth. In columns (B) to (H) are shown the images predicted by the analyzed methods with dimension 256 $\times$ 256.

TABLE II: Training hyperparameters.

Parameter	Value
image size	256 $\times$ 256
learning rate	0.001
batch size	20
epoch	25
dropout probability	0.3
optimizer	Adam
loss method	binary crossentropy
early stopping patience	12

of training of a U-Net, showing the accuracy, F1 Score, and Jaccard Index. As can be seen, the validation set metrics converged.

Table III presents the average values of the metrics for the 9 combinations of browning indices and segmentation methods. The table also exhibits the U-Net results and their combinations with browning indices. The results in the table are ordered in descending order of the F1 Score values.

We can observe in Table III that the best result was achieved when combining U-Net with the three browning indices. This composition obtained F1 Score and Jaccard Index around 6% and 13%, respectively, superior to the same metrics of the U-Net with RGB images. The experiments carried out with the brown index BI_{Fetuga} showed noise in the segmentation. This could mean that it was less efficient in enhancing the lesion than the other two indices. This could mean that the formulation of the browning index $BI_{Fetuga} = 100 - L$ in the color space in L*a*b* is not suitable for brown colored lesions. On the other hand, Aimonino browning index was, in general, the best BI. The combination of Aimonino + Otsu achieved some results close to those of U-Net, which is an approach much more complex. Based on the rates obtained, we can state that using Aimonino browning index is suitable in the case of brown lesions.

Figure 6 shows a dermatoscopic image, the ground truth, and the results obtained after applying the browning index techniques.

Experiments were also carried out with images of dimension 512 $\times$ 512, but similar results were obtained for each method, with the drawback that training a U-Net with images with this dimension takes more time and memory.

V. Conclusions

This article aimed to propose a methodology to segment skin melanoma lesions using three Browning Indices (BI), $BI_{aimonino}$, $BI_{Lunadei_2}$, and BI_{Fetuga}. As a baseline method, results achieved only using U-Net deep neural network were compared to those obtained with U-Net and the use of Browning Indices BIs.

The best results were obtained when a U-Net was trained with images composed of three browning indices. When compared with the usual method of training U-Net with RGB images, this combination of methods returned F1 Score and Jaccard Index around 6% and 13% higher, respectively. Even simpler approaches, such as Aimonino + Otsu, returned F1 Score close to that obtained by U-Net with RGB images. These results indicate the potential of the browning indices to aid skin lesion segmentation.

This topic will be further explored by checking other deep learning based approaches combined with browning indices in order to improve skin lesion segmentation and classification. We also intend to combine the browning indices with approaches that extract information from the contours of skin lesions to increase the quality of skin lesion classification, since skin cancer spot has irregular contours.

Acknowledgment

The authors acknowledge the financial support given by CNPq (Conselho Nacional de Desenvolvimento Científico e Tecnológico) and FAPES (Fundação de Amparo à Pesquisa do Espírito Santo), numbers 598/2018 and 02/2019.

References

[1] Li, Y. and Shen, L. (2018). Skin lesion analysis towards melanoma detection using deep learning network. Sensors (Switzerland), 18.

[2] WHO (2017). World health organisation - radiation: Ultraviolet (uv) radiation and skin cancer. Who, 9.

TABLE III: Comparative results between Browning Index & Threshold with image 256 $\times$ 256.

Method	Jaccard Index	Accuracy	F1-Score
(Aimonino,Fetuga,Lunadei) + U-Net	**0.719**	**0.917**	**0.862**
Aimonino + U-Net	0.611	0.901	0.808
U-Net	0.594	0.889	0.805
Lunadei + U-Net	0.578	0.892	0.792
Aimonino + Otsu	0.671	0.782	0.776
Aimonino + Watershed	0.667	0.841	0.772
Lunadei + Otsu	0.658	0.773	0.763
Lunadei + Watershed	0.655	0.832	0.761
Aimonino + Lloyd	0.643	0.806	0.759
Lunadei + Lloyd	0.619	0.802	0.738
Fetuga + U-Net	0.371	0.858	0.665
Fetuga + Lloyd	0.445	0.717	0.570
Fetuga + Otsu	0.436	0.715	0.561
Fetuga + Watershed	0.431	0.768	0.555

[3] do Nascimento, M. I., de Moraes, J. R. F. C., Silva, E. R. C., da Mota, M. G. G., and Guimarães, R. M.(2021). Tendências na mortalidade por câncer de pele não melanoma no brasil e suas macrorregiões. Revista Brasileira de Cancerologia, 68.

[4] Zhang, R. (2021). Melanoma detection using convolutional neural network. 2021 IEEE International Conference on Consumer Electronics and Computer Engineering, ICCECE 2021.

[5] Lunadei, L., Galleguillos, P., Diezma, B., and Lie, L.(2010). Evaluation of enzymatic browning in fresh-cut apple slices applying a multispectral vision system. In International Conference on Agricultural Engineerig. AgEng, pages 1–11, 2010.

[6] Gaede, G. M. and Facon, J. (2020). Data Augmentation Novo em Redes Neurais Convolucionais. In Anais Eletrônicos da Jornada de IC da Ufes, pages 1–14, 2020.

[7] Barbosa, S. R. and Facon, J. (2020). Aplicações em Segmentacão de Padrões Marrons. In Anais Eletrônicos da Jornada de IC da Ufes, pages 1–15, 2020.

[8] Aimonino, D. R., Barge, P., Comba, P. G., Occelli, A., and Tortia, C. (2015). Computer Vision for Laboratory Quality Control on Frozen Fruit. In Chemical Engineering Transactions, volume 44, pages 1–6, 2015.

[9] Fetuga, G., Tomlins, K., and Henshaw, F. (2014). Effect of variety and processing method on functional properties of traditional sweet potato flour (“elubo”) and sensory acceptability of cooked paste (“amala”). In Master thesis, Federal University Of Agriculture, Abeokuta, 2014.

[10] Codella N, Gutman D, Celebi ME, Helba B, Marchetti MA, Dusza S, Kalloo A, Liopyris K, Mishra N, Kittler H, Halpern A (2017). Skin Lesion Analysis Toward Melanoma Detection: A Challenge at the 2017 International Symposium on Biomedical Imaging (ISBI), Hosted by the International Skin Imaging Collaboration (ISIC). arXiv: 1710.05006 [cs.CV]

[11] Ly, B. C. K., Dyer, E. B., Feig, J. L., Chien, A. L., and Bino, S. D. (2020). Research techniques made simple: Cutaneous colorimetry: A reliable technique for objective skin color measurement. Journal of Investigative Dermatology, 140.

[12] Long, J., Shelhamer, E., and Darrell, T.. Fully Convolutional Networks for Semantic Segmentation, arXiv e-prints, 2014. doi:10.48550/arXiv.1411.4038.

[13] Ronneberger, O., Fischer, P., Brox, T. (2015). U-Net: Convolutional Networks for Biomedical Image Segmentation. In: Navab, N., Hornegger, J., Wells, W., Frangi, A. (eds) Medical Image Computing and Computer-Assisted Intervention – MICCAI 2015. MICCAI 2015. Lecture Notes in Computer Science, vol 9351. Springer, Cham. doi: 10.1007/978-3-319-24574-4_28.

[14] Cassidy, B., Kendrick, C., Brodzicki, A., Jaworek- Korjakowska, J., and Yap, M. H. (2022). Analysis of the isic image datasets: Usage, benchmarks and recommendations. Medical Image Analysis, 75.

[15] Otsu, N. (1979). Threshold selection method from graylevel histograms. IEEE Trans Syst Man Cybern, SMC-9.

[16] F. Morii, A supervised Lloyd algorithm and segmentation of handwritten Japanese characters, 9th European Signal Processing Conference (EUSIPCO 1998), Rhodes, Greece, 1998, pp. 1-4.

[17] Y. Wu and Q. Li, The Algorithm of Watershed Color Image Segmentation Based on Morphological Gradient, Sensors, vol. 22, no. 21, p. 8202, Oct. 2022, doi: 10.3390/s22218202.